This is a preprint version of the following published document: Dalton Transactions, 2013, 42, 15774-15784. DOI: https://doi.org/ 10.1039/C3DT51708J

Supramolecular aggregates of metallo-organic acids with stilbazoles. Formation of columnar mesophases and Langmuir films.

Cristina Domínguez,[a,b] *Bertrand Donnio,*[b,c] *Silverio Coco,**[a] *and Pablo Espinet,**[a]

[a] IU CINQUIMA/Química Inorgánica, Facultad de Ciencias, Universidad de Valladolid, 47071 Valladolid, Castilla y León, Spain. [b] Institut de Physique et Chimie des Matériaux de Strasbourg (IPCMS), UMR 7504 (CNRS-Université de Strasbourg), 23 rue du Loess, BP 43, F-67034 Strasbourg Cedex 2 (France). [c] Complex Assemblies of Soft Matter Laboratory (COMPASS), UMI 3254 (CNRS-Rhodia/Solvay-University of Pennsylvania), CRTB, 350 George Patterson Boulevard, Bristol, PA 19007 (USA).

This is a preprint version of the following published document: Dalton Transactions, 2013, 42, 15774-15784. DOI: https://doi.org/ 10.1039/C3DT51708J

Table of contents

Supramolecular complexes formed through hydrogen bonding between tris(3,4,5-decyloxy)stilbazole and various metallo-organic acids have been synthesized, revealing the potential of this system to build functional liquid crystals and Langmuir films.

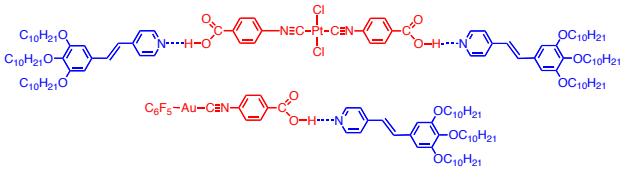

Abstract

Supramolecular metal complexes formed through hydrogen bonding between tris(3,4,5-decyloxy)stilbazole and several metallo-organic acids of the types [Au(R)($CNC_6H_4CO_2H$)], (R = C_6F_5, $C_6F_4OC_{10}H_{21}$), [*cis*-[$MCl_2(CNC_6H_4COOH)_2$] and [*trans*-[$MI_2(CNC_6H_4COOH)_2$] (M = Pd, Pt) have been synthesized. All the supramolecular palladium and platinum polycatenar aggregates display a hexagonal columnar mesophase at temperatures close to room temperature. Most of the supramolecular trisalkoxystilbazole complexes exhibit luminescent behaviour. Aggregates of [Au($C_6F_4OC_{10}H_{21}$)($CNC_6H_4CO_2H$)] and [*trans*-[$MI_2(CNC_6H_4COOH)_2$] (M = Pd, Pt) form stable Langmuir films at the air-water interface.

Keywords: Isocyanide, Stilbazole, Gold, Palladium, Platinum, Hydrogen bond, Liquid crystals, Langmuir films, Luminescence.

Introduction

Intermolecular hydrogen bonding is one of the key attractive interactions stabilizing condensed phases and promoting molecular self-assembly. The ability to modulate H-bonded arrays opens interesting opportunities for the rational design of nanostructures with useful physical or chemical properties.[1] Intermolecular hydrogen bonding has been employed to obtain organic liquid crystals, gelators, well-defined nanometer-scale or mesoscopic assemblies, thin films, and polymeric materials that self-assemble from simple elementary units.[2] As far as liquid crystals are concerned, small molecules such as 4-alkoxybenzoic acids show liquid crystalline behaviour as a consequence of their self-assembling into dimers, which enhances the overall molecular anisotropy, *via* hydrogen

bonds.[3,4] But the importance of intermolecular hydrogen bonding in liquid crystals is not limited to this simple seminal example, it has been observed in many other diverse situations. [5,6,7,8,9,10,11,12,13,14,15,16,17,18,19,20,21] However, in the field of metal-containing liquid crystals,[4,22] only a few metallomesogens are based on intermolecular hydrogen-bonded complexes. These are: a few hydrogen-bonded ferrocene complexes;[23,24,25] phenanthroline copper derivatives;[26] pyrazole rhodium complexes;[27] salicyladimine derivatives of palladium, copper and vanadium;[28] dicyanometallate-based networks combined with dicationic tectons;[29] and some 4-isocyanobenzoic acid metal complexes reported by our group. [30,31,32]

In our initial studies, we found that 4-isocyanobenzoic acid metal complexes (metallo-organic acids) of the type [AuXCNC$_6$H$_4$COOH] (X = halogen, fluoroaryl) and *trans*-[MI$_2$(CNC$_6$H$_4$COOH)$_2$] (M = Pd, Pt) can act as proton donors to decyloxystilbazole, giving rise to supramolecular metal complexes displaying liquid crystalline behaviour.[30,31] Such decyloxystilbazole based aggregates have a rod-like structure and display smectic and nematic phases. Their thermal stability at high temperatures was low because of the lability of the hydrogen bond at the transition temperatures required for that system. In this regard, the use of triazines as proton acceptors that can form intermolecular double hydrogen bonds with carboxylic acids has allowed us to obtain stable supramolecular aggregates of 2,4,6-triarylamino-1,3,5-triazine with the carbonyl metallo-organic acids such as [Fe(CNC$_6$H$_4$COOH)(CO)$_4$] and [M(CNC$_6$H$_4$COOH)(CO)$_5$] (M = Cr, Mo, W).[32]

An obvious strategy to achieve more thermally stable metallomesogens of this type is to reduce the transition temperatures of the system, which can be achieved by connecting a larger number of terminal alkoxy substituents into the molecule, as in polycatenar liquid

crystals.[33] Using this strategy produces important structural changes in the system, generating pseudo-disk-like or tapered-like molecules likely to self-assemble into columns, and to drive the formation of columnar mesophases. This is, of interest for organic-based electronic applications,[34] such as organic light-emitting diodes, field-effect transistors, and photovoltaics.[34,35,36]

The self-organizing properties of liquid crystals can also be used to produce highly ordered and stable monolayers at the air–water interface (Langmuir films). Many studies in this field have been carried out on discotic flat conjugated molecules that form columnar structures, such as triphenylenes,[37] or some families of metallomesogens with N-donor ligands, such as phthalocyanines,[38] and porphyrins.[39]

On these grounds, we decided to investigate the ability of trisalkoxystilbazoles to act as proton-acceptors towards several metallo-organic acids derived from 4-isocyanobenzoic acid and to form supramolecular molecules that might behave as metallomesogens, and be potentially useful to prepare Langmuir films. The interest of these systems is that the aggregates formed by hydrogen bonding are able to "swallow" the metallic fragment into an aliphatic environment very efficiently, when arranged in columnar mesophases, even for pretty bulky and unfavourable metal geometries. The disguised metal will then acquire properties, still little explored for this kind of systems, more typical of organic molecules. One could think, for instance, of using these systems as shuttles for a metal to penetrate the cell membrane. We report here on various supramolecular metal complexes formed through hydrogen bonding between tris(3,4,5-decyloxy)stilbazole and the various metallo-organic acids of the type $[Au(R)(CNC_6H_4CO_2H)]$, (R = C_6F_5, $C_6F_4OC_{10}H_{21}$), [*cis*-$[MCl_2(CNC_6H_4COOH)_2]$ and [*trans*-$[MI_2(CNC_6H_4COOH)_2]$ (M = Pd, Pt) . The latter type

of supramolecular hexacatenar aggregates affords new examples of supramolecular metallomesogens that display a hexagonal columnar mesophase. Most of the supramolecular trisalkoxystilbazole aggregates display luminescence, and the adducts with $[Au(C_6F_4OC_{10}H_{21})(CNC_6H_4CO_2H)]$, and [*trans*-$[MI_2(CNC_6H_4COOH)_2]$ (M = Pd, Pt) form stable Langmuir films at the air-water interface.

Results and Discussion

Synthesis and characterization

The set of hydrogen-donating metallo-organic acids used in this study includes $[CNC_6H_4CO_2H]$ **(1)**,[30] $[AuX(CNC_6H_4CO_2H)]$ (X = Cl **(2)**,[30] C_6F_5 **(3)**,[31] $C_6F_4OC_{10}H_{21}$) **(4)**, $[\mu\text{-}C_6F_4C_6F_4\text{-}\{AuCNC_6H_4CO_2H\}_2]$ **(5)**,[31] *cis*-$[MCl_2(CNC_6H_4CO_2H)_2]$ [(M = Pd **(6)**, Pt **(7)**] and *trans*-$[MI_2(CNC_6H_4CO_2H)_2]$ [M = Pd **(8)**, Pt **(9)**].[30] The tetrafluorophenyl complex **(4)**, not prepared previously, was obtained from $[Au(C_6F_4OC_{10}H_{21})(tht)]$ (tht: tetrahydrothiophene) and 4-isocyanobenzoic acid, as reported for similar perfluorophenylgold complexes.[31]

The hydrogen-bonded acid-stilbazole complexes were synthesized by dissolving together stoichiometric amounts of tris(decyloxy)stilbazole and the corresponding monocarboxylic and dicarboxylic metallo-organic acids (i.e. in 1:1 and 2:1 molar proportions respectively), in tetrahydrofuran at room temperature, and subsequently evaporating the solvent under vacuum (Scheme 1). Compared to the white or pale yellow acidic and stilbazole precursors, the supramolecular stilbazole aggregates are intense yellow solids, or reddish waxy solids in the case of dichloropalladium and platinum

complexes, This colour change supports the formation of supramolecular stilbazole complexes by hydrogen bonding, as reported for similar systems.[40,41] Besides the colour change, the formation of the supramolecular adducts was ultimately confirmed by the changes observed in the IR spectrum when compared to the parent metallo-organic acids (Table 1, discussed below).

Thus, the treatment of the gold compounds [AuCl($CNC_6H_4CO_2H$)] **(2)** and [μ-$C_6F_4C_6F_4$-{Au($CNC_6H_4CO_2H$)}$_2$] **(5)** with trisalkoxystilbazole do not display any significant variation of their ν(C≡N), ν(C=N) and ν(C=O) absorptions, revealing that the corresponding tris(decyloxy)stilbazole supramolecular complexes **S2** and **S5** do not form. The lower solubility of both [AuCl($CNC_6H_4CO_2H$)] and [μ-$C_6F_4C_6F_4$-{Au($CNC_6H_4CO_2H$)}$_2$], compared with the other metallo-organic acids, is the most likely reason for their failure to form supramolecular aggregates.

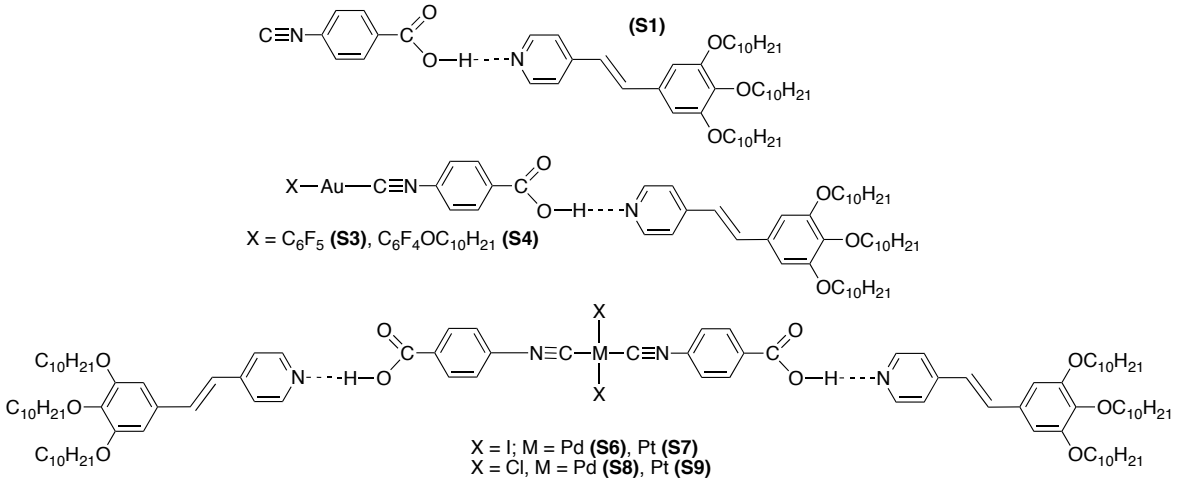

Scheme 1. Molecular structures of the various metallo-organic H-bonded complexes.

However, the formation of the hydrogen-bonded tris(decyloxy)stilbazole supramolecular complexes in the solid state was confirmed by IR spectroscopy (Table 1 and SI) for all other materials. For these, the infrared spectra show the absorption band of the stilbazole group at 1585 cm^{-1}, corresponding to ν(C=N) vibrations, shifted to higher wavenumbers than their parent complexes, as reported for nitrophenol-alkoxystilbazole aggregates.[42] The presence of unreacted material can be safely excluded, even when the ν(C=O) band from the carboxylic group appears only slightly shifted from their position in the parent complexes. These changes, together with the fact that the stilbazole aggregates are more coloured than their parent precursors, confirm that the self-association of the metallo-organic acids has been replaced by intermolecular hydrogen-bond to the stilbazole, as reported for other supramolecular aggregates formed by combining various benzoic acids and stilbazoles.[43]

Table 1. Selected infrared spectral data in KBr Pellets (cm^{-1}) for the metallo-organic acids and their stilbazole aggregates.

		4-isocyanobenzoic acid (**1**), and free metallo-organic acids (**2-9**)		Stilbazole (**S**) and stilbazole aggregates (**S1-S9**)		
Compound		ν(C≡N)	ν(C=O)	ν(C≡N)	ν(C=N)	ν(C=O)
Tris(decyloxy)stilbazole	**(S)**				1581	
$[CNC_6H_4COOH]$	**(1)**	2128	1702	2119	1600	1703
$[AuCl(CNC_6H_4CO_2H)]$	**(2)**	2239	1695	2240	1580	1695
$[Au(C_6F_5)(CNC_6H_4CO_2H)]$	**(3)**	2216	1701	2215	1606	1700
$[Au(C_6F_4OC_{10}H_{21})(CNC_6H_4CO_2H)]$	**(4)**	2210	1686	2209	1606	1700
$[\mu\text{-}C_6F_4C_6F_4\text{-}\{AuCNC_6H_4CO_2H\}_2]$	**(5)**	2206	1691	2206	1580	1691
$[PdI_2(CNC_6H_4CO_2H)_2]$	**(6)**	2193	1698	2191	1609	1700
$[PtI_2(CNC_6H_4CO_2H)_2]$	**(7)**	2186	1697	2185	1608	1703

$[PdCl_2(CNC_6H_4CO_2H)_2]$	**(8)**	2242 (sh) 2220 (s)	1696	2191	1608	1700
$[PtCl_2(CNC_6H_4CO_2H)_2]$	**(9)**	2243 (m) 2206 (s)	1696	2197	1610	1703

sh = shoulder; s = strong; m = medium.

All supramolecular trisalkoxystilbazole complexes display the corresponding isocyanide ν(C≡N) bands in the same region of their parent complexes.[30] The *cis* metallo-organic acid precursors display two ν(C≡N) absorptions, while the *trans* derivatives show only one, as expected on symmetry grounds.[44] The **S6** and **S7** aggregates show one ν(C≡N) absorption, as their *trans*-$[MI_2(CNC_6H_4COOH)_2]$ [M = Pd (**6**), Pt (**7**)] precursors, confirming that the *trans* arrangement of the ligands is maintained in the aggregate. However, in contrast to their *cis*-$[MCl_2(CNC_6H_4COOH)_2]$ [M = Pd (**8**), Pt (**9**)] precursors, **S8** and **S9** show only one C≡N band, which appears at lower wavenumbers than for **8** and **9** (Figure 1), revealing that the formation of **S8** and **S9** involves a *cis-trans* isomerization.[45] It should be noted that IR spectra of **S8** and **S9** recorded in the mesophase are almost identical to the IR spectra of the material in the solid state, supporting that the supramolecular aggregates persist in the mesophase.

This is a preprint version of the following published document: Dalton Transactions, 2013, 42, 15774-15784. DOI: https://doi.org/ 10.1039/C3DT51708J

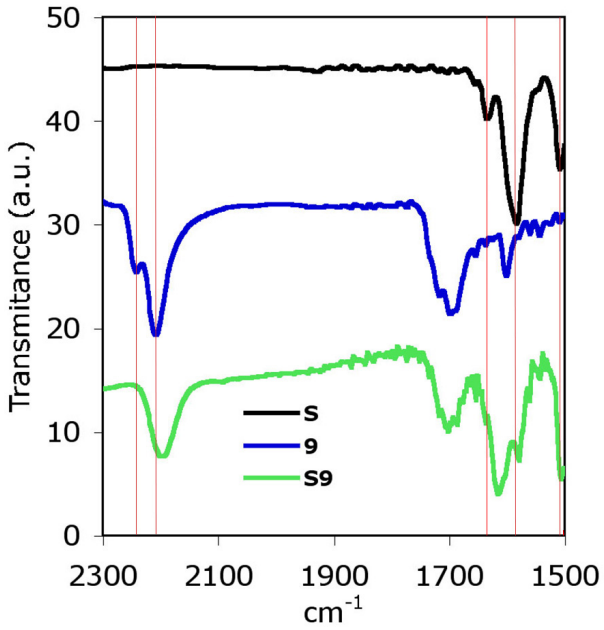

Figure 1. FTIR spectra of free stilbazole (**S**), the metallo-organic acid (**9)**, and the stilbazole aggregate (**S9)**. Red lines are to facilitate comparison of the spectra.

The metal-containing stilbazole aggregates have only low stability in solution and diffusion-ordered NMR spectroscopy (DOSY-NMR) support that the acid metallic fragments and the stilbazole are dissociated not only in d^8-THF but also in the non-coordinating solvent CD_2Cl_2.

Thermal and mesomorphic behaviour.

Optical, thermal and thermodynamic data are collected in Table 2. The thermal behaviour of all the complexes was studied by polarized optical microscopy (POM), differential scanning calorimetry (DSC), and small-angle X-ray scattering (SAXS) experiments. While tris(decyloxy)stilbazole (**S**),[46] all the metallo-organic acids (**1-9**), and the supramolecular aggregates obtained from gold (**S3** and **S4**) are not liquid crystals, the four hexacatenar,

square-planar palladium and platinum aggregates (**S6-S9**) display a thermotropic liquid-crystalline behaviour: both the "MCl_2" derivatives show a mesophase at or slightly above room temperature, while for the "MI_2" complexes, a mesophase appears above 40-70°C, up to *ca*. 120-140°C. When observed under POM, the four complexes display clearly a liquid crystal texture, although their features do not allow to identify unambiguously the mesophase formed by this technique only, and SAXS experiments were required. On heating, a weakly birefringent and homogeneous texture was nevertheless observed for the MCl_2 complexes from the melting temperature to about 110-120 ºC, when the transition to the isotropic liquid occurred; just before melting, the samples did not appear homogeneous, with the entanglement of hard and soft zones. On cooling from the isotropic liquid (**S8** and **S9**), weakly birefringent patterns, though not typical, were also observed upon mechanical shear (Figure 2), down to room temperature, where still no crystallization was detected, even after several hours. The same behaviour is observed by DSC, suggesting that the frozen material is keeping the order of the mesophase (glassy liquid-crystalline phase). Such an assumption for this complex solid state behaviour is not unrealistic, and it is frequently observed for hexacatenar mesogens and other intricate molecular architectures, due to the retardation of the crystallization processes, and to the high tendency for these compounds to evolve towards frozen mesomorphic states. Moreover, these materials are very viscous and the aryl conformations relative to the average from one molecule to another can change generating micro domains. Thus, for these compounds one should expect a wide interval of temperatures with coexistence of two phases (a kind of conformational hysteresis) for any transition, as observed in dendrimers and in chain-

disordered polymers. Consequently it is not unexpected than the clearing temperatures are not detected by DSC.

Unlike the chloro derivatives, the iodo complexes suffer extensive decomposition at temperatures close to their clearing. This produces non-reversibility of their thermal cycles when these include isotropization.

Table 2. Optical, thermal and thermodynamic data of tris(decyloxy)stilbazole aggregates.

Metalloacid-stilbazole adducts		Transition[a]	T[b] (ºC)	ΔH[b] (kJ/mol)
Tris(decyloxy)stilbazole	**(S)**	Cr → I	54	92.9
$[CNC_6H_4CO_2H)]$	**(S1)**	Cr → I	68[c]	
$[Au(C_6F_5)(CNC_6H_4CO_2H)]$	**(S3)**	Cr → Cr'	46	8.1
		Cr' → Cr''	66	28.0
		Cr'' → I	100	67.8
$[Au(C_6F_4OC_{10}H_{21})(CNC_6H_4CO_2H)]$	**(S4)**	Cr → I	43	63.6
$[PdI_2(CNC_6H_4CO_2H)_2]$	**(S6)**	Cr+ $gCol_h$ → Col_h	40-60	10.7
		Col_h → I + dec.	120-140	30.3[d]
$[PtI_2(CNC_6H_4CO_2H)_2]$	**(S7)**	Cr+ $gCol_h$ → Col_h	24-65	11.7[d]
		Col_h → I + dec.	120-140	72.5[d]
$[PdCl_2(CNC_6H_4CO_2H)_2]$	**(S8)**	$gCol_h$ → Col_h	30-50[c]	(-)
		Col_h → I	119[c]	(-)
$[PtCl_2(CNC_6H_4CO_2H)_2]$	**(S9)**	$gCol_h$ → Col_h	50-60[c]	(-)
		Col_h → I	110-115[c]	(-)

[a] Cr-Cr", crystalline phases; $gCol_h$, glassy columnar hexagonal phase; Col_h, columnar hexagonal phase; I, isotropic liquid; dec., decomposition. [b] Data referred to the first DSC cycle starting from the crystal. [c] Microscopic data on first heating. [d] Combined enthalpies (clearing transition + decomposition).

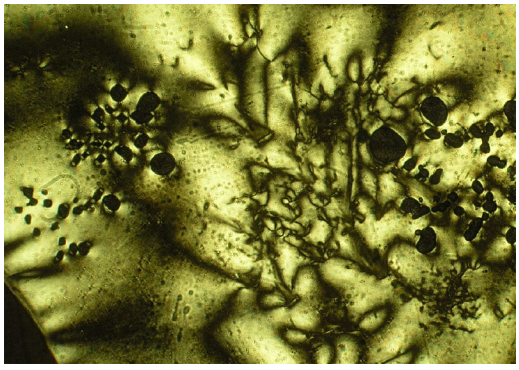

Figure 2. Polarized optical microscopic texture (x100) observed for **S9** (chosen as a representative example) upon cooling from the isotropic liquid at 104 ºC.

X-ray diffraction experiments.

Temperature-dependent X-ray diffraction experiments (SI) were carried out in order to unambiguously identify the nature of the mesophase. Structural data from X-ray diffraction experiments are collected in Table 3. X-ray patterns in the pristine state for **S6** and **S7** show four reflections in the ratio 1:2:3:√12 and several sharp reflections in the large-angle range, in perfect agreement with a crystalline hexagonal lattice (same ratio, and similar periodicities as the Col mesophase). In addition, a weak halo embedding the sharp reflection can be observed revealing the presence of a small fraction of the same structure, but in glassy state (SI). Thus, at room temperature **S6** and **S7** are partially crystalline. In contrast **S8** and **S9** show the Col mesophase at room temperature, but in its frozen state. Above the transition temperatures, long-time acquisition (typically between 2 and 6 hours) temperature-dependent X-ray patterns appeared however detrimental to the complexes integrity, particularly to the iodo derivatives (**S6** and **S7**) essentially due to their low thermal stability at high temperatures (e.g. 100°C). Indeed, in some situations, X-ray patterns revealed co-existence of a mesophase (sharp small-angle reflections, and broad large-angle scatterings) and a crystalline phase (sharp reflections in the mid- and wide-angle range (i.e. $10° < 2\theta < 30°$), ascribed to mixtures of the precursory components (not liquid at these temperatures) and remaining small aggregates, confirming that the complexes likely dissociate at such temperatures. Thus, only short acquisition times were considered (*ca.* maximum 30 minutes of exposure) for the SAXS experiments in the

mesophases. Under these experimental conditions, diffraction patterns with a few sharp small-angle peaks (**S8** and **S9**), and only one for the iodo compounds **(S6** and **S7)**, along with two diffuse scatterings in the mid- and low-angle range, with maxima at ca. 8.5-9.0 and at 4.5 Å respectively, were obtained, which confirmed mesophases formation and also permitted their complete characterizations.

Table 3. Indexation of the reflections and structural parameters of the hexagonal columnar (Col_h) phases obtained from small-angle X-ray diffraction experiments.

Metallo-organic acid stilbazole complexes T/ºC		Indexation			Parameters[d]
	d_{meas}/Å[a]	*hk*[b]	I[c]	d_{calc}/Å[a]	
(S6) T = 80, 120 ºC	45.85 8.8 4.5	10	VS (sh) W (br) VS (br)	45.85 h_{mol} h_{ch}	a = 52.9 Å S = 2425 Å^2 V_{mol} = 3500±100 Å^3 $N_h \approx 6$ for h = h_{mol}
(S7) T = 80, 120 ºC	44.8 9.0 4.5	10	VS (sh) W (br) VS (br)	44.8 h_{mol} h_{ch}	a = 51.7 Å S = 2315 Å^2 V_{mol} = 3500±100 Å^3 $N_h \approx 6$ for h = h_{mol}
(S8) T = 60 ºC	43.5 25.3 16.5 14.6 8.5-9.0 4.5	10 11 21 30	VS (sh) M (sh) VW (sh) VW (sh) W (br) S (br)	43.7 25.23 16.52 14.57 h_{mol} h_{ch}	a = 50.45 Å S = 2205 Å^2 V_{mol} = 3200±100 Å^3 $N_h \approx 6$ for h = h_{mol}
(S9) T = 80 ºC	42.4 24.5 16.0 14.2 8.5-9.0 4.5	10 11 21 30	VS (sh) M (sh) VW (sh) W (br) S (br)	42.45 24.51 16.05 14.15 h_{mol} h_{ch}	a = 49.0 Å S = 2080 Å^2 V_{mol} = 3100±100 Å^3 $N_h \approx 6$ for h = h_{mol}

[a] d_{meas} and d_{calc} stand for measured and calculated periodicity. [b] Miller indices, *hk*; [c] I corresponds to the intensity of the reflections (VS : very strong, S: strong, M: medium, W: weak; br and sh stand for broad and sharp); h_{ch} represents the molten chain short-range distance and h_{mol} represents a short-range periodicity of the strongly scattering metallic centres. [d] Phase parameters: Col_h, lattice parameter, $a = 2\times[\Sigma d_{hk}\sqrt{(h^2+k^2+hk)}]/N_{hk}\sqrt{3}$; number of reflections, N_{hk}; columnar cross-section of the hexagonal cell, $S = \frac{1}{2}a^2\sqrt{3}$; V_{mol}, molecular volume, is determined considering a density of *ca*. 1 g.cm^{-3}, according to $MW/(6.022.10^{23})(10^{-24})$, where MW is the molecular weigh. N_h is the number of molecular equivalent per one fictitious columnar repeat unit h-thick, according to $N_h = h\times SV_{mol}$.

The X-ray patterns of **S8** complex, recorded at 60 ºC, exhibit two sharp and intense and two weaker low-angle diffraction peaks, of decreasing intensity as a function of increasing diffracting angles, with reciprocal d spacings in the 1:√3:√7:√9 ratio. These features are unambiguously assigned to the (10), (11), (21) and (30) reflections of a hexagonal columnar phase with a lattice parameter, a = 50.45Å (Figure 3).[47] The broad low- and wide-angle signals (h_{mol}, h_{ch}) were associated to some weakly correlated intermolecular distances i.e. a short-range periodicity between strongly scattering metallic centres and to the molten aliphatic chains, respectively. **S9** displayed a similar diffraction pattern with reciprocal d spacings in a 1:√3:√7:√9 ratio, assigned to the same set of reflections of the Col_h phase (a = 49.0 Å, Figure 3).

In both cases, the fundamental reflection (10) is the most intense and clearly dominates the diffraction pattern over the weak harmonics and higher-order reflections. Moreover, the reflection intensity decay with diffraction angles is also particularly abrupt. Both features reveal the strong confinement at the nodes of the hexagonal lattice of the electron-rich mesogenic cores incorporating the highly scattering metallic ionic fragments within the columnar cores, and separated by an electron-poor medium formed by the molten chains. This strong contrast within the electronic density modulation, decreasing abruptly from the central core to the periphery, and the larger core volume fraction with respect to that of the chain, are at the origin of the particular and substantial enhancement of the fundamental reflection (10) intensity with respect to the other reflections and to the diffuse scattering h_{ch}. X-ray patterns for the derivatives **S6** and **S7** only exhibit one single, sharp but very intense fundamental small-angle reflection. The absence of harmonics and higher orders of the hexagonal lattice, as well as the lightly intense halo h_{ch}, are also the result of both the

enhancement of the electronic density at the nodes of the lattice and likely the weaker chemical segregation between the rigid and soft parts, and thus less well-defined interfaces du to increase molecular volume, all contributing simultaneously to the attenuation of their intensity, at least below the detection limits within this experimental setup. Considering that these metal complexes have the same molecular structures as **S8** and **S9**, it can reasonably be assumed that they most likely show the same mesophase, namely a Col_h phase with phase parameters a = 52.9 and 51.7 Å, respectively, with a slight lattice expansion of ca. 2.5 Å with respect to those of the chloro derivatives, **S8** and **S9**, in consistency with the larger size of the iodine co-ligands.

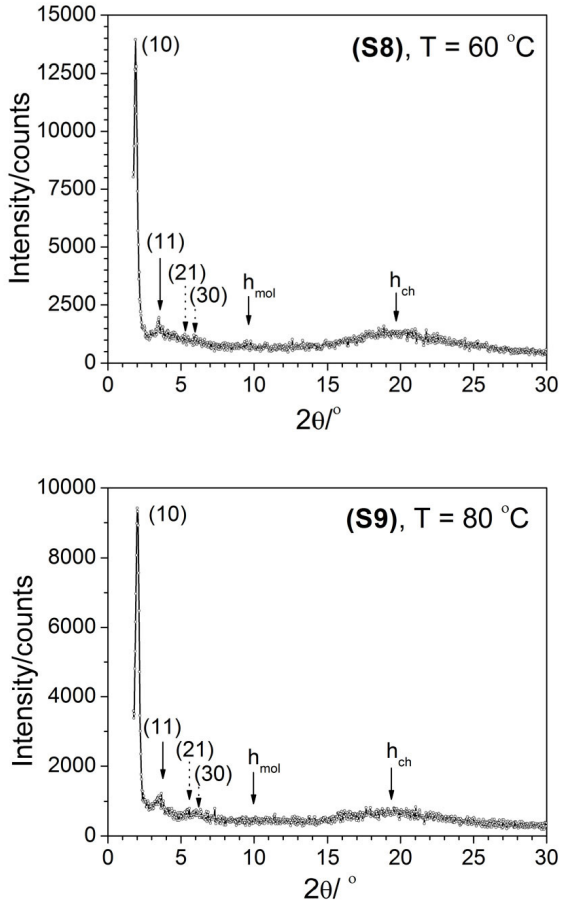

Figure 3. X-ray diffraction patterns of the Col_h phase of **S8** and **S9** recorded at 60 and 80 °C.

As commonly observed with hexacatenar mesogens,[33] the four complexes exhibit a single type of columnar mesophase, which has been assigned to as Col_h. However, similarly to structurally related polycatenar metallomesogens.[48] the diameter of the columns in the Col_h phases (i.e. the a-lattice parameter) is significantly smaller than the estimated molecular length of the complexes (about 65.9 Å with fully extended conformation of the chains), assuming that the linear *trans* arrangements of the isocyanide ligands and of the stilbazoles

are preserved in the mesophase. This implies that the complexes cannot lie in the lattice plane as do purely organic homologues (for which the molecular lengths match the lattice parameters[33]), but rather display a significant tilt of their main molecular axis (approximately in the 30-50° range) with respect to the columnar axis (Scheme 2). This tilt issue is not incompatible with the need for the columns to have a circular cross-section perpendicular to the columns direction, required in the case of *p6mm* symmetry of the Col_h phase, providing that the tilt of the rigid molecular cores is appropriate. As previously reported,[44d] it is postulated here too that the supramolecular arrangement within the columnar phase is also driven by the hexagonal symmetry of the Col_h mesophase, one of the most efficient way to fill the available space, and thus that the rigid mesogenic cores must be tilted at some specific angles with respect to the lattice plane to accommodate this symmetry and that the segregating diverging hydrocarbon chains will be sufficiently mobile and liquid-like to efficiently fill the available volume around the cylindrical columnar cores (Scheme 2). Obviously, for symmetry consistency, the tilt directions are not correlated from one column to its neighbours (and the tilt is either not necessarily within one single column), which would, in the contrary, lead to the reduction of the phase symmetry. An estimation of the molecular density within a fictitious columnar "slice" can be deduced considering the short-range periodicity along the columnar axis, h_{mol}: this result shows that the occupancy along a stretch of column of ca. 9 Å thick is about six molecular equivalents (Table 3), and that the value of the columnar cross-section area is compatible with the projection on the lattice plane of about three complexes (Scheme 2).

For these supramolecular complexes the data are consistent with three molecules (or molecular equivalents) and, as do structurally related hexacatenars, the adducts must pack

in flat supramolecular bundles (3 complexes side-by-side) within columnar layers of 4.5 Å thick along the columnar axis on average. The signal h_{mol}, at about twice the distance h_{ch}, may imply a different orientation of the adjacent molecular bundles, and therefore, assuming that the linear coordination of the *trans* arrangements of the isocyanide ligands is preserved in the mesophase, it is probable that neighbouring molecules thus will stack with random rotations (with respect to neighbouring molecules) and tilts (with respect to the lattice plane), so that the hydrocarbon chains fill efficiently the peripheral space around the columnar core, and yield columns with an average cylindrical shape.

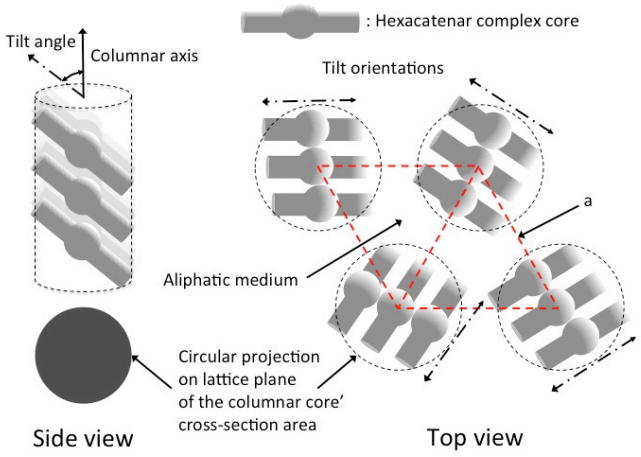

Scheme 2. Schematic representation of the self-assembling of the complexes within cylindrical columns, and their self-organization within the *p6mm* Col_h mesophase.

Photoluminescence studies

The luminescent properties of the supramolecular stilbazole-acid aggregates have been studied in the solid state, where the H-bonded aggregates are maintained. The luminescence spectroscopic data of the supramolecular stilbazole-acid aggregates are listed in Table 4.

All the stilbazole aggregates, except the diiodo palladium and platinum compounds **S6** and **S7,** are luminescent and display a yellow–green luminescence visually observed under UV irradiation at 365 nm. All the emission spectra are similar and consist of one emission band with the maximum in the range 449-545 nm. The free isocyanide ligand is weakly luminescent in the solid state showing an emission band involving π---π* intraligand-localized states.[31] The parent gold metalloacid complexes **3-4** are luminescent too, showing one strong emission band associated with the presence of intermolecular Au---Au interactions.[31] On the contrary, the dihalobisisocyanide palladium- and platinum complexes **6-9** do not display luminescent behaviour, probably due to the absence of extensive metallophilic interactions in their structures, as reported for similar complexes of palladium and platinum with arylisocyanides.[49]

The stilbazole used as proton acceptor is luminescent and shows a fluorescent emission band with a maximum at 449 nm, which is assigned to π---π* localized transitions by analogy with similar stilbazole systems.[50] It is well known that formation of H-bonded aggregates based on stilbazole derivatives produces a strong bathochromic shift of the emission maximum compared to the free stilbazole,[50,51] in keeping with our experimental results (Table 4). On the other hand, all the emission spectra of the luminescent aggregates are similar, in spite of the very different nature of the acids used. This strongly suggests that luminescence of the H-bonded aggregates is based on stilbazole localized transitions.

Table 4. Emission (λ_{em}) and excitation (λ_{ex}) maxima (in nm) for the stilbazole adducts at 298 K.

KBr

Metalloacid-stilbazole adducts		λ_{ex}	λ_{em}
Tris(decyloxy)stilbazole	**(S)**	389	449
$[CNC_6H_4CO_2H)]$	**(1)** [31]	353	469
$[CNC_6H_4CO_2H)]$	**(S1)**	335	496
$[Au(C_6F_5)(CNC_6H_4CO_2H)]$	**(S3)**	395	497
$[Au(C_6F_4OC_{10}H_{21})(CNC_6H_4CO_2H)]$	**(S4)**	494	528
$[PdI_2(CNC_6H_4CO_2H)_2]$	**(S6)**	-	-
$[PtI_2(CNC_6H_4CO_2H)_2]$	**(S7)**	-	-
$[PdCl_2(CNC_6H_4CO_2H)_2]$	**(S8)**	468	546
$[PtCl_2(CNC_6H_4CO_2H)_2]$	**(S9)**	462	545

Aggregate **S8** was chosen as a representative example for variable-temperature monitoring of the luminescence. The excitation and emission spectra of **S8** were recorded from 25 to 130 °C (Figure 4). The pattern of the spectra is similar to that obtained in KBr dispersion, as reported for other isocyanide complexes.[52] The intensity decreases as the temperature increases, but the overall profile of the spectra is maintained even beyond the clearing transition to the isotropic liquid state (119 °C), which supports an intramolecular origin of the emission,[53] as suggested above. The process is reversible, and the intensity of the emission is gradually recovered upon cooling.

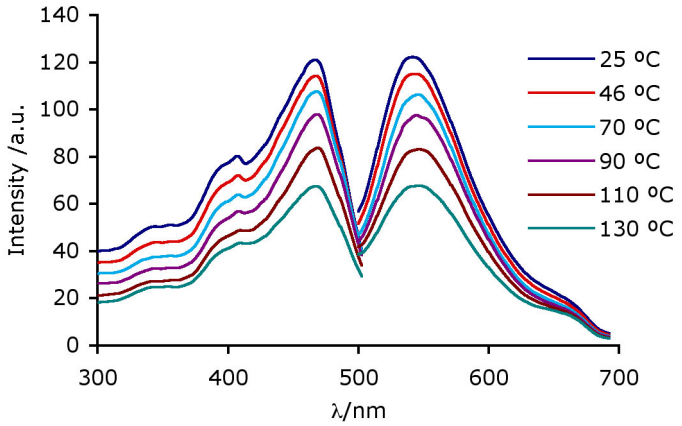

Figure 4. Luminescence excitation and emission spectra of **S8** at different temperatures, heating from 25 to 110 ºC. The spectra and the temperature list follow the same top to bottom order.

Langmuir Films

The free stilbazole (**S**) and the supramolecular aggregates **S4, S6 and S7** form Langmuir films at the air-water interface. The isotherms obtained at 25 ºC and the molecular areas extrapolated to zero surface pressure are shown in Figure 5. The surface pressures vary from 0 mN/m^{-1} until the collapse of the film occurs at pressures between 20 mN/m^{-1} for **S4** and 50 mN/m^{-1} for **S6.**

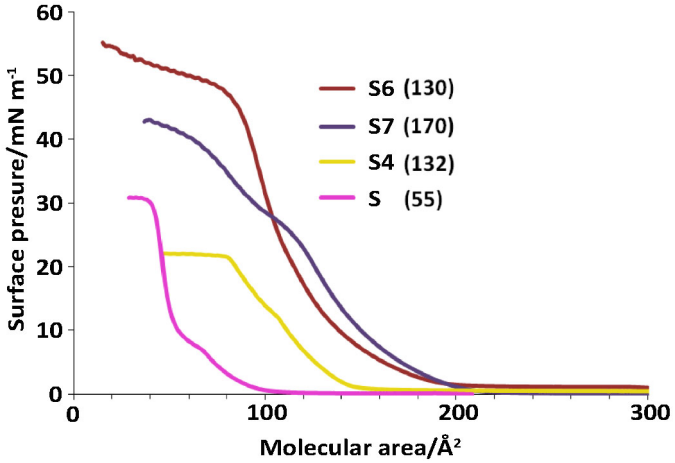

Figure 5. Surface pressure-molecular area isotherms at 25 ºC. Extrapolated molecular area is given in brackets (Å^2).

Brewster angle microscopy (BAM) was used to study the homogeneity of the films. The free stilbazole (**S**) and **S4**, **S6** and **S7** complexes form a liquid film that, upon compression, becomes continuous and non defective (Figure 6).

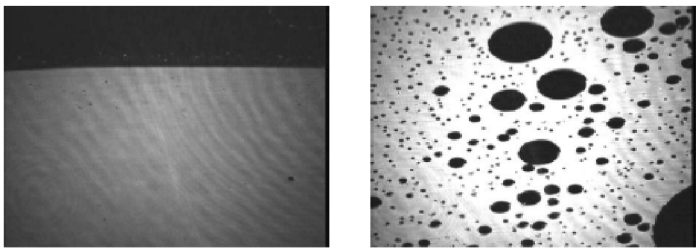

Figure 6. BAM images (620 x 500 μm) obtained during the compression of the Langmuir film of: (a) **S** at A = 210 Å^2, (b) **S4** at A = 200 Å^2. For **S6** and **S7** see Figure SI1 (SI).

The molecular area found for the free stilbazole **(S)** is 55 Å^2, which is in good agreement with the area estimated considering a cross section of 20-25 Å^2 per alkoxy chain,[54] for a monolayer in which the molecules are arranged perpendicularly to the water interface. In contrast, the area found for the gold complex **S4** (132 Å^2) is very similar to the estimated value for the area of the molecular core, (gold-coordinated core plus stilbazole, 130 Å^2), which suggests that the molecules are arranged parallel to the water surface (side-on disposition) with the alkoxy substituents normal to the film surface (Figure 7). The collapse of the film is produced at a low pressure, suggesting a low stability of this film. BAM images of a film when approaching collapse are collected in Figure SI2 (SI).

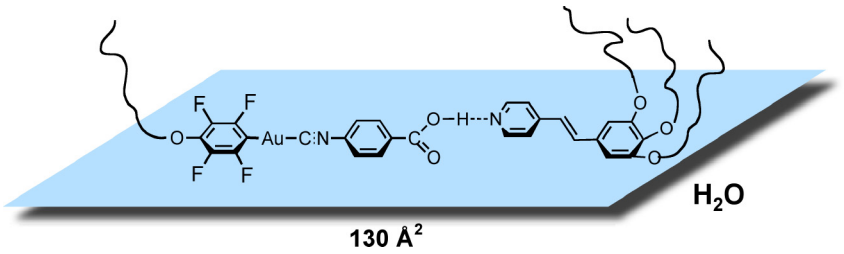

Figure 7. Proposed schematic representation for the monolayer of the **S4** aggregate.

The influence of the number of alkoxy substituents of the stilbazole fragment on the film formation was examined. The isotherm of the related mesomorphic supramolecular complex [Au($C_6F_4OC_{10}H_{21}$)(CNC_6H_4COOH)(decyloxystilbazole)],[31] which has only one alkoxylic chain in the stilbazole group, indicates an area of 70 $Å^2$ per molecule, which is in between end-on and side-on molecular arrangement. BAM images (Figure 8) show the formation of an inhomogeneous film with birefringent microdomains, displaying a *Schlieren* texture (Figure 8d) similar to that displayed by this compound in bulk, in its smectic C mesophase. This suggests that the molecular arrangement in the SmC mesophase and in these microdomains is the very similar.

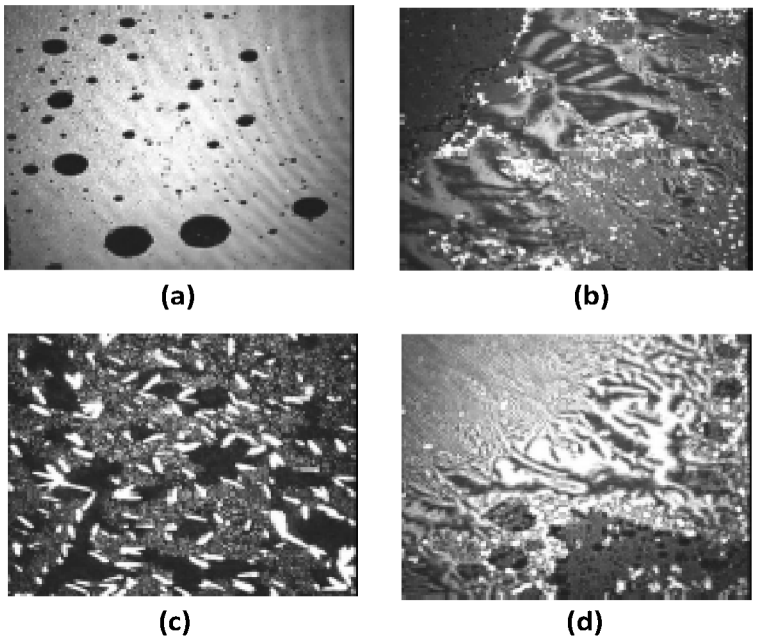

Figure 8. BAM images (620 x 500 μm) obtained during the compression-decompression cycles of the Langmuir film of [Au($C_6F_4OC_{10}H_{21}$)(CNC_6H_4COOH)-4-decyloxystilbazole] at ($Å^2$/molecule): (a) 109, (b) 56, (c) 35, (d) 60. A more complete sequence is collected in figure SI3 (SI).

This is a preprint version of the following published document: Dalton Transactions, 2013, 42, 15774-15784. DOI: https://doi.org/ 10.1039/C3DT51708J

The molecular area found for the stilbazole supramolecular complexes **S6** (130 $Å^2$) and **S7** (170 $Å^2$) is smaller than expected for a molecular arrangement parallel to the water surface (side-on disposition) and the alkoxy substituents normal to the film surface, but is also much larger than expected for an edge-on orientation. Since the hydrogen bonds in these systems are not strong, it is not unlikely that the supramolecular complex could easily dissociate in a mixture of its components. From the X-ray diffraction data of *trans*-$[PdI_2(CNC_6H_4CO_2H)_2]$ and those of the film obtained for stilbazole, the molecular area found for two molecules of stilbazole plus one molecule of *trans*-$[PdI_2(CNC_6H_4CO_2H)_2]$ is *ca.* 140 $Å^2$, which supports an edge-on orientation of the three fragments that constitute the supramolecular aggregate **S6** (Figure 9), in a similar orientation as described for 16-hydroxy stearic acid.[55]

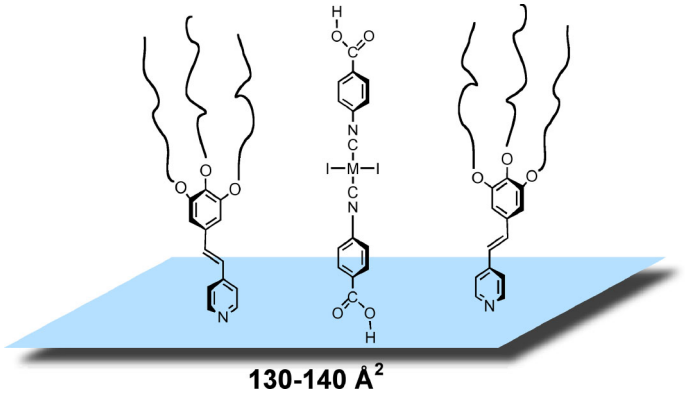

Figure 9. Proposed schematic representation for the monolayer of the **S6** aggregate.

The collapse of the film occurs at a pressure higher than 40 $mN{\cdot}m^{-1}$, thus indicating a good cohesion of the monolayer and a good anchoring of the molecules on the water surface. This is reflected in BAM images where, at high pressures, the film it is observed to fold and then break (Figures 10 and SI4).

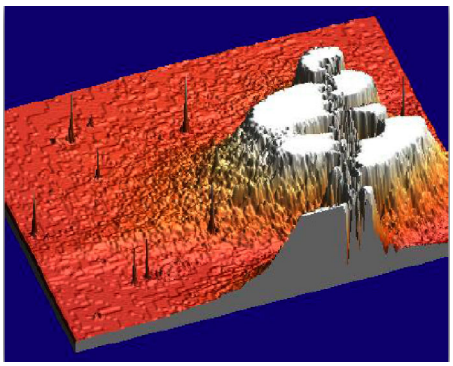

Figure 10. Three-dimensional representation of BAM image (Figure SI4b) of **S6** obtained during collapse of film at 90 $Å^2$.

It is important to note that pure *trans*-[$PdI_2(CNC_6H_4CO_2H)_2$] does not form Langmuir films. The BAM images show that only solid aggregates are formed (Figure SI5), probably due to lack of the alkoxy chains and the strong acid-acid interactions. Consequently, the combination of metalloacid and stilbazole is the key point for the formation of the monolayer.

In summary, this study shows the potential and limitations of the metallo-organic acid-stilbazole interactions to build liquid crystals and little studied Langmuir films. For Pd and Pt the aggregates formed through hydrogen bonding are stable enough to behave as a single metal-organic molecule with a defined shape. They self-arrange into columns with the metal fragment inside the column, and give rise to columnar mesophases, but are fragile on the water surface, which splits the aggregates and liberates their component fragments distributed perpendicular to the water surface in the stable LB films formed. For Au the presence of three chains of the trisalkoxystilbazole is not enough to induce columnar

mesophases but, remarkably, the hydrogen bond survives on the water surface giving rise to films with the molecules arranged parallel to the water surface.

Acknowledgments. This work was sponsored by the Ministerio de Ciencia e Innovación (Project CTQ2011-25137) and the Junta de Castilla y León (Project VA248A11-2). C. D. thanks the Ministerio de Ciencia e Innovación for a studentship and Drs Jean-Louis Gallani and Mircea-Vasile Rastei (IPCMS) for their help in the Langmuir-Blodgett studies. B. D. thanks the CNRS and the University of Strasbourg for support.

Experimental

Combustion analyses were made with a Perkin-Elmer 2400 microanalyzer. IR spectra (cm^{-1}) were recorded on a Perkin-Elmer FT BX instrument and ^{1}H and ^{19}F NMR spectra on Bruker AV-400 instrument in $CDCl_3$. Microscopy studies were carried out using a Leica DMRB microscope equipped with a Mettler FP82HT hot stage and a Mettler FP90 central processor, at a heating rate of 10 °C min^{-1}. For differential scanning calorimetry (DSC) a Perkin-Elmer DSC7 instrument was used, which was calibrated with water and indium. The scanning rate was 10 °C min^{-1}, the samples were sealed in aluminum capsules in the air, and the holder atmosphere was dry nitrogen. Emission and excitation spectra were measured at 298 K in the solid state as finely pulverized KBr mixtures in quartz tubes, or in the mesophase by means of a remote fiber optic accessory (and the Mettler FP-82HT hot stage) with a Perkin-Elmer LS-55 spectrofluorometer. The XRD patterns were obtained by transmition diffraction with a Guinier experimental set-up. A linear focalized

monochromatic Cu-Kα_1 beam (λ = 1.5405 Å) was obtained using a sealed-tube generator (900 W) equipped with a bent quartz monochromator. In all cases, the crude powder was filled in thin Lindemann capillaries of 1 mm diameter and 10 μm wall-thickness, in air (corrections for air were made), and then heated to produce the mesophase. An initial set of diffraction patterns was recorded with a curved Inel CPS 120 counter gas-filled detector linked to a data acquisition computer; periodicities up to 70 Å can be measured, and the sample temperature controlled to within ±0.01 °C from 20 to 200°C. Alternatively, patterns were also recorded on an image plate; periodicities up to 120 Å can be measured (scanned by STORM 820 from Molecular Dynamics with 50μm resolution). In each case, exposure times were varied from 1 to 24 h.

Langmuir films were prepared on a standard TEFLON® trough filled with ultrapure water at room temperature. The compounds were dissolved in chloroform or in a mixture chloroform/tetrahydrofurane (4:1) in 1 $mg{\cdot}cm^{-3}$ concentration to prepare the spreading solution. The monolayers were compressed at a constant speed of 7 $mm{\cdot}min^{-1}$

Brewster angle microscopy observations were performed with an apparatus from NFT (Göttingen, Germany, www.nanofilm.de).

Literature methods were used to prepare [$CNC_6H_4CO_2H$], [$AuX(CNC_6H_4CO_2H)$] (X = Cl, C_6F_5), [μ-$C_6F_4C_6F_4$-{$AuX(CNC_6H_4CO_2H)$}$_2$], [$MX_2(CNC_6H_4CO_2H)_2$] (M = Pd, Pt, X = Cl, I), and tris(decyloxy)stilbazole.[46]

Preparation of [Au($C_6F_4OC_{10}H_{22}$)(C≡NC_6H_4COOH)]. To a solution of [$HC_6F_4OC_{10}H_{22}$] (0.38 mmol) in 25 mL of dry diethyl ether was added dropwise a solution of LiBun in hexane (0.26 mL, 0.38 mmol) at -78 ◦C, under nitrogen. After stirring for one

hour at -50 ◦C, solid [AuCl(tht)] (0.123 g, 0.38 mmol) was added at -78 ◦C and the reaction mixture was slowly brought to room temperature (3 h). Then, a few drops of water were added and the solution was filtered in air through anhydrous MgSO4. [C≡NC$_6$H$_4$OOH] (0.056 g, 0.38 mmol) was added to the solution obtained. After stirring for 1 h, the solvent was removed on a rotary evaporator and the white solid obtained was recrystallized from THF/hexane at -15 ◦C. Yield: 0.081 g, 33%. Anal. Calcd for $C_{24}H_{16}AuF_4NO_3$: C, 44.38; H, 4.04; N, 2.16 %. Found: C, 44.18; H, 4.02; N, 2.54%. IR (cm^{-1}/KBr): ν(C≡N): 2211, ν(C=O): 1680. IR (cm^{-1}/(THF): ν(C≡N): 2218, ν(C=O): 1724, 1707. 1H NMR (THF-d$_8$): δ 8.2 (d, *J* = 8.3 Hz, 2H), 7.9 (d, *J* = 8.3 Hz, 2H), 4.12 (t, *J* = 6.4 Hz, 2H), 1.50–1.25 (m, 16H), 0.91 (t, *J* = 7.02 Hz, 3 H). ^{19}F NMR (THF-d$_8$): -118.4 (m, 2F), -158.2 (m, 2F).

Preparation of hydrogen-bonded supramolecular complexes. The supramolecular complexes were prepared from the pure components. Exact stoichiometric molar amounts of the two compounds were dissolved in dry tetrahydrofuran at room temperature, and the solvent was pumped off in vacuum, affording the aggregates as intense yellow solids or reddish waxy solids (supramolecular derivatives of *cis*-palladium and platinum metallo-organic acids).

Electronic Supplementary Information. BAM images, elemental microanalysis for the aggregates, IR spectra and DSC scans, and X-Ray diffractograms.

References

[1] (*a*) M. Muthukumar, C. K. Ober, E. L. Ober and E. L. Thomas, *Science,* 1997, **277**, 1225-1232; (*b*) S. I. Stupp and P. V. Braun, *Science,* 1997, **277**, 1242-1248; (*c*) Z.-R. Chen, J. A. Kornfield, S. S. Smith, J. T. Grothaus and M. M. Satkowski, *Science,* 1997, **277**, 1248-1253; (*d*) R. C. Smith, W. M. Fischer and D. L. Gin, *J. Am. Chem. Soc*., 1997, **119**, 4092-4093; (*e*) S. A. Miller, E. Kim, D. H. Gray and D. L. Gin, *Angew. Chem., Int. Ed*., 1999, **38**, 3021-3026.

[2] (*a*) J. H. K. K. Hirschberg, L. Brunsveld, A. Ramzi, J. A. J. M. Vekemans, R. P. Sijbesma and E. W. Meijer, *Nature,* 2000, **407**, 167-170; (*b*) P. Jonkheijm, A. Miura, M. Zdanowska, F. J. M. Hoeben, S. De Feyter, A. P. H. J. Schenning, F. C. De Schryver and E. W. Meijer, *Angew. Chem., Int. Ed*., 2004, **4**, 74-78; (*c*) C. Tschierske, *Prog. Polym. Sci*., 1996, **21**, 775-852; (*c*) T. Kato, *Struct. Bonding,* 2000, **96**, 95-146; (*d*) H.-K. Lee, H. Lee, Y. H. Ko, Y. J. Chang, N.-K. Oh, W.-C. Zin and K. Kim, *Angew. Chem., Int. Ed*., 2001, **40**, 2669-2671; (*e*) I. Yoshikawa, J. Li, Y. Sakata and K. Araki, *Angew. Chem., Int. Ed*., 2004, **43**, 100-103; (*f*) P. Terech and R. G. Weiss, *Chem. Rev.,* 1997, **97**, 3133-3160.

[3] G. W. Gray*, Molecular Structure and Liquid Crystals*, Academic Press, London, 1967, p. 161, and references therein.

[4] *Handbook of Liquid Crystals*, eds. D. Demus, J. W. Goodby, G. W. Gray, H. W. Spiess, V. Vill, Wiley-VCH: Weinheim, 1998.

[5] T. Kato and J. M. J. Fréchet, *J. Am. Chem. Soc.,* 1989, 8533-8534.

[6] U. Kumar, T. Kato and J. M. J. Fréchet, *J. Am. Chem. Soc.,* 1992, 6630-6639.

[7] M.-J. Brienne, J. Gabard, J.-M. Lehn and I. Stibor, *J. Chem. Soc. Chem. Commun*., 1989, 1868-1870.

[8] K. Willis, D. J. Price, H. Adams, G. Ungar and D. W. Bruce, *J. Mater. Chem.,* 1995, **5,** 2195-2199.

[9] C. M. Paleos and D. Tsiourvas, *Liq. Cryst.,* 2001, **28**, 1127-1161.

[10] C. M. Paleos and D. Tsiourvas, *Angew. Chem. Int. Ed. Engl*., 1995, 34, 1696-1711.

[11] M. Grunert, R. A. Howie, A. Kaeding and C. T. Imrie, *J. Mater. Chem*., 1997, **7**, 211-214.

[12] F. Würthner, S. Yao, B. Heise and C. Tschierske, *Chem. Commun*., 2001, **14**, 2260-2261.

[13] N. Mizoshita, H. Monobe, M. Inoue, M. Ukon, T. Watanabe, Y. Shimizu, K. Hanabusa and T. Kato, *Chem. Commun*., 2002, **15**, 428-429.

[14] S. Jin, Y. Ma, S. C. Zimmerman and S. Z. D. Cheng, *Chem. Mater*., 2004, **16**, 2975-2977.

[15] T. Kajitani, S. Kohmoto, M. Yamamoto and K. Kishikawa, *Chem. Mater*., 2004, **16**, 2329-2331.

[16] J. Barberá, L. Puig, P. Romero, J. L. Serrano and T. Sierra, *Chem. Mater*., 2005, **17**, 3763-3771.

[17] J. A. McCubbin, X. Tong, Y. Zhao, V. Snieckus and R. P. Lemieux, *Chem. Mater*., 2005, **17***,* 2574-2581.

[18] K.-U. Jeong, S. Jin, J. J. Ge, B. S. Knapp, M. J. Graham, J. J. Ruan, M. M. Guo, H. M. Xiong, F. W. Harris and S. Z. D. Cheng, *Chem. Mater*., 2005, **17***,* 2852-2865.

[19] J. Barberá, L. Puig, P. Romero, J. L. Serrano and T. Sierra, *J. Am. Chem. Soc.,* 2006, **128**, 458-464.

[20] B. Gündogan and K. Binnemans, *Liquid Crystals*, 2000, **27**, 851-858.

[21] Y. Xu, W. Qu, Q. Yang, J. Zheng, Z. Shen, X. Fan and Q. Zhou, *Macromolecules,* 2012, **45***,* 2682-2689.
[22] D. W. Bruce, *Inorganic Materials*; 2nd Edition, eds. D. W. Bruce and D. O'Hare, Wiley: Chichester, 1996, ch. 8.
[23] R. Deschenaux, F. Monnet, E. Serrano, F. Turpin and A.-M. Levelut, *Helv. Chim. Acta,* 1998, **81**, 2072-2077.
[24] P. Massiot, M. Imperór-Clerc, M. Veber and R. Deschenaux, *Chem. Mater*., 2005, **17***,* 1946-1951.
[25] B. Donnio, J. M. Seddon and R. Deschenaux, *Organometallics,* 2000, **19**, 3077-3081.
[26] R. Ziessel, G. Pickaert, F. Camerel, B. Donnio, D. Guillon, M. Cesario and T. Prangé, *J. Am. Chem. Soc.,* 2004, **126**, 12403-12413.
[27] R. Giménez, A. Elduque, J. A. López, J. Barberá, E. Cavero, I. Lantero, L. A. Oro and J. L. Serrano, *Inorg. Chem*., 2006, **45,** 10363-10370.
[28] (*a*) S.-Y. Li, C.-J. Chen, P.-Y. Lo, H.-S. Sheu, G.-H. Lee and C. K. Lai, *Tetrahedron*, 2010, **66,** 6101-6112; (*b*) Y. J. Wang, J. H. Song, Y. S. Lin, C. Lin, H. S. Sheu, G. H. Lee and C. K. Lai, *Chem. Commun*., 2006, 4912-4914.
[29] P. Dechambenoit, S. Ferlay, B. Donnio, D. Guillon and M. W. Hosseini, *Chem. Commun*., 2011, **47**, 734-736.
[30] S. Coco, E. Espinet, P. Espinet and I. Palape, *Dalton Trans.,* 2007, 3267-3272.
[31] S. Coco, C. Cordovilla, C. Domínguez and P. Espinet, *Dalton Trans.,* 2008, 6894-6900.
[32] S. Coco, C. Cordovilla, C. Domínguez, B. Donnio, P. Espinet and D. Guillon, *Chem. Mater.,* 2009, **21**, 3282–3289.
[33] H.-T. Nguyen, C. Destrade and J. Malthête, *Adv. Mater*., 1997, **9**, 375-388.
[34] (*a*) B. R. Kaafarani, *Chem. Mater*., 2011, 378-396; (*b*) W. Pisula, M. Zorn, J. C. Chang, K. Müllen and R. Zentel, *Macromol. Rapid Commun*., 2009, **30**, 1179-1202; (*c*) T. Kato, T. Yasuda and Y. Kamikawa, *Chem. Commun.,* 2009, 729-739; (*d*) S. Sergeyev, W. Pisula and Y. H. Geerts, *Chem. Soc. Rev.,* 2007, **36**, 1902-1929; (*e*) S. Laschat, A. Baro, N. Steinke, F. Giesselmann, C. Hägele, G. Scalia, R. Judele, E. Kapatsina, S. Sauer, A. Schreivogel and M. Tosoni, *Angew. Chem., Int. Ed*., 2007, **46**, 4832-4887.
[35] (*a*) A. W. Hains, Z. Liang, M. A. Woodhouse and B. A. Gregg, *Chem. Rev.,* 2010, **110**, 6689-6735; (*b*) M. Oukachmih, P. Destruel, I. Seguy, G. Ablart, P. Jolinat, S. Archambeau, M. Mabiala, S. Fouet and H. Bock, *Sol. Energy Mater. Sol. Cells,* 2005, **85**, 535-543; (*c*) L. Schmidt-Mende, A. Fechtenkötter, K. Müllen, E. Moons, R. Friend and J. MacKenzie, *Science,* 2001, **293**, 1119-1122.
[36] B. Roy, N. De and K. C. Majumdar, *Chem. Eur. J.,* 2012, **18**, 14560-14588.
[37] (*a*) D. Goldmann, D. Janietz, R. Festag, C. Schmidt and J. H. Wendorff, *Liq. Cryst*., 1996, **21**, 619-623; (*b*) J. Y. Josefowicz, N. C. Maliszewskyj, S. H. J. Idziak, P. A. Heiney, J. P. McCauley and A. B. Smith III, *Science,* 1993, **260**, 323-326; (*c*) D. Gidalevitz, O. Y. Mindyuk, P. A. Heiney, B. O. Ocko, M. L. Kurnaz and D. K. Schwartz, *Langmuir,* 1998, **14**, 2910-2915; (*d*) P. Henderson, D. Beyer, U. Jonas, O. Karthaus, H. Ringsdorf, P. A. Heiney, N. C. Maliszewskyj, S. S. Ghosh, O. Y. Mindyuk and J. Y. Josefowicz, *J. Am. Chem. Soc.,* 1997, **119**, 4740-4748; (*e*) A. Tolkki, E. Vuorimaa, V. Chukharev, H. Lemmetyinen, P. Ihalainen, J. Peltonen, V. Dehm and F. Würthner, *Langmuir,* 2010, **26**, 6630-6637.

[38] J. Simon and P. Bassoul, *Phthalocyanines: Properties and Applications*, vol. 2, eds. C. C. Leznoff and A. B. P. Lever, VCH: Weinheim, 1993, p. 227.
[39] P. Facci, M. P. Fontana, E. Dalcanale, M. Costa and T. Sacchelli, *Langmuir,* 2000, **16**, 7726-7730.
[40] This color change has been suggested to be due to the shift of the absorption band of stilbazole chromophore as a consequence of the hydrogen bond formation: D. W. Bruce, *Adv. Inorg. Chem.,* 2001, **52**, 151-204.
[41] A. Ryabchun, A. Bobrovsky, V. Shibaev, S. Gromov, N. Lobova and M. Alfimov, *J. Photochem. Photobiol. A: Chem.,* 2011, **221**, 22-29.
[42] D. J. Price, K. Willis, T. Richardson, G. Ungar and D. W. Bruce, *J. Mater. Chem.*, 1997, **7**, 883-891.
[43] D. W. Bruce, *Adv. Inorg. Chem.,* 2001, **52**, 151-204.
[44] B. Crociani, T. Boshi and V. Belluco, *Inorg. Chem.,* 1970, **9**, 2021.
[45] S. Coco, F. Díez-Expósito, P. Espinet, C. Fernández-Mayordomo, J. M. Martín-Álvarez, and A. M. Levelut, *Chem. Mater.* 1998**, 10***,* 3666-3671.
[46] B. Donnio and D. W. Bruce, *New J. Chem.*, 1999, 275-286.
[47] A.-M. Levelut, *J. Chim. Phys*., 1983, **80**, 149.
[48] (*a*) B. Donnio and D. W. Bruce, *J. Chem. Soc. Dalton Trans.,* 1997*,* 2745-275; (*b*) J. F. Eckert, U. Maciejczuk, D. Guillon and J. F. Nierengarten, *Chem. Commun.,* 2001*,* 1278-1279; (*c*) L. Plasseraud, L. González Cuervo, D. Guillon, G. Süss-Fink, R. Deschenaux, D. W. Bruce and B. Donnio, *J. Mater. Chem*., 2002, **12***,* 2653-2658; (*d*) B. Donnio, B. Heinrich, H. Allouchi, J. Kain, S. Diele, D. Guillon and D. W. Bruce, *J. Am. Chem. Soc*., 2004, **126***,* 15258-15268; (*e*) M. J. Mayoral, C. Rest, V. Stepanenko, J. Schellheimer, R. Q. Alburquerque and G. Fernández, *J. Am. Chem. Soc.,* 2013, **135**, 2148-2151. (*f*) R. W. Date, E. Fernández-Iglesias, K. E. Rowe, J. M. Elliott, D. W. Bruce, *Dalton Trans*. 2003, 1914–1931.
[49] (*a*) I. M. Sluch, A. J. Miranda and L. M. Slaughter, *Cryst. Growth Des*., 2009, **9**, 1267-1270; (*b*) I. M. Sluch, A. J. Miranda, O. Elbjeirami, M. A. Omary and L. M. Slaughter, *Inorg. Chem*., 2012, **51**, 10728-10746.
[50] A. Ryabchun, A. Bobrovsky, V. Shibaev, S. Gromov, N. Lobova and M. Alfimov, *J. Photochem. Photobiol. A: Chem.,* 2011, **221**, 22-29.
[51] H.-C. Lin, C-M. Tsai, G.-H. Huang and Y.-T. Tao, *Macromolecules,* 2006**, 39***,* 557-568.
[52] R. Bayón, S. Coco and P. Espinet, *Chem. Eur. J.,* 2005, **11**, 1079-1085.
[53] J. Arias, M. Bardají and P. Espinet, *Inorg. Chem.,* 2008, **47**, 3559-3567.
[54] A. Ulman, *Ultrathin Organic Films*, Academic Press Inc.: New York, 1991.
[55] A. Dhathathreyan, *Colloids and Surfaces A: Physicochem. Eng. Aspects*, 2008, **318**, 307-314.